Anisotropic Metasurface-Based Beam-Scanning Dual-Polarized Fan-Beam Integrated Antenna System

Kranti Kumar Katare, *Student Member, IEEE*, Sandhya Chandravanshi, *Student Member, IEEE*, Abhishek Sharma, *Member, IEEE*, Animesh Biswas, *Senior Member, IEEE*, and M. Jaleel Akhtar, *Senior Member, IEEE*

***Abstract*— This paper presents a novel anisotropic metasurface (AMS)-based integrated antenna system to facilitate dual-polarized fan-beam patterns with independent beam-scanning ability. In the proposed configuration, the antenna subsystem comprises a specially designed differentially fed microstrip patch antenna (source antenna) along with a polarization rotator (PR). The differential antenna arrangement is realized using a square shaped microstrip patch capacitively coupled with two metallic strips, which are connected to a specially designed wideband hybrid coupler using two metallic vias for the microstrip feeding. This source antenna is loaded with a PR by placing it at a height of $0.35\lambda_0$ from the radiating aperture. The PR comprised two identical metallic layer patterns, separated by two substrates. Depending upon the relative orientation of these layers, the polarization of the linearly polarized impinging spherical electromagnetic (EM) waves (originating from the source antenna) either remains preserved or gets rotated by 90° while transmitting through this PR. After realizing the antenna subsystem, a novel AMS lens is designed and placed above the PR. The proposed AMS lens is realized by integrating two cylindrical MS (CMS) lenses, CMS_Y and CMS_X. This integration provides a unique phase profile to the AMS lens, thus introducing appropriate phase correction to the incident orthogonally polarized spherical EM waves along their respective polarization direction. The proposed configuration of AMS lens, thus, results into formation of the independent dual-polarized fan-beam radiation beams. Finally, the steering of the generated fan-beams along the direction of their respective polarization is facilitated using the proposed system by translating the AMS lens parallel to the source antenna.**

***Index Terms*— Anisotropic metasurface (AMS), beam-scanning, capacitive coupling, cylindrical phase profile, differential feed, dual-polarized, fan-beam, hybrid coupler, polarization rotator (PR).**

I. Introduction

IN MANY applications such as the airborne collision avoidance system, the resolution in the azimuth plane is more critical than in the elevation plane (or vice versa). Under these situations, the fan-beam-like pattern is more effective than the pencil-beam pattern in order to facilitate fast scanning of the target area [1]. The antennas with fan-beam radiation patterns are also demanded for various applications such as the imaging [2], [3], the satellite communication [4], the wireless communication [5], and the radar detection [6]. These antennas are especially required in the radar configurations like pulse radar [1], the Doppler weather radar [7], the automotive radar [8], and the scanning millimeter wave radar [9]. In the fan-beam pattern, the half-power beamwidth along the azimuth and elevation planes are different and its ratio varies from 2 to 25, as per the system requirement [10]. In order to achieve the fan-beam-type radiation pattern, different configurations based on the reflector antenna [2]–[4], the antenna array [1], [5], the dielectric lens antenna [11], just to name a few, have been reported in the literatures. However, problem of radiation blockage in reflector antennas and high losses in the feed structure of antenna array may deteriorate the overall performance of these kinds of antenna configurations. Although the antenna configuration reported in [11] mitigates these shortcomings (radiation blockage and feed losses) up to certain extent, the complex design process of the dielectric lens involving different dielectric materials seems less attractive from the implementation point of view due to various fabrication constraints. Apart from the requirement of the fan-beam-type radiation pattern, most of the point-to-multipoint communications, the aircraft landing, the RF imaging, and the radar configurations preferably use dual-polarized antennas in order to avoid any interference at the transmitting/receiving stations [2], [3]. In these kind of configurations, dual-polarized fan-beam-type radiation patterns have usually been obtained in the past by utilizing two separate antenna systems, resulting into overall bulky configuration. In order to facilitate effective communication between the transmitting and the receiving antennas in all types of situations, the inclusion of scanning capability using the single antenna for such kinds of dual-polarized fan-beam antenna configurations appears to be quite desirable.

It is investigated in this work that the dual-polarized fan-beam compact antenna system with beam-scanning capability can easily be realized by utilizing the transmission-type metasurface (MS)-based lens structure. An MS inspired lens structure basically modulates the phase of the impinging electromagnetic (EM) waves and, thus, radiation beams with different shapes such as pencil-beam, multiple-beam, or fan-beam can be obtained [12], [13]. Recently, numerous structures based on MS lens have been reported to focus the radiation beam either into a single direction using the pencil-beam pattern [14]–[16] or along multiple directions using the multiple-beam pattern [17]. In order to tilt and further steer the direction of pencil-beam pattern, the MS structures with high transmission/reflection characteristic have

Manuscript received March 6, 2019; revised May 23, 2019; accepted June 21, 2019. Date of publication July 30, 2019; date of current version November 27, 2019. *(Corresponding author: Kranti Kumar Katare.)*

The authors are with IIT Kanpur, Kanpur 208016, India (e-mail: krantikatarerf@gmail.com).

Color versions of one or more of the figures in this article are available online at http://ieeexplore.ieee.org.

Digital Object Identifier 10.1109/TAP.2019.2930128

also been presented [18]–[22]. From the above discussion, it can be inferred that the simple MS-based lens structures have been employed in the past for processing the pencil-beam pattern. However, they have not been widely utilized for generation and steering of the fan-beam pattern. Moreover, the reported MS-based structures were usually polarization independent and, hence, their response is not suitable for obtaining the dual-polarized configuration. Therefore, a new kind of polarization-sensitive MS that is an anisotropic MS (AMS) is investigated in this work for obtaining dual-polarized configuration. This AMS (also known as the birefringent MS) can actually be used to control the amplitude and the phase of the impinging EM waves depending upon their polarization state [23]. It should be noted here that the previously reported AMS-based configurations have primarily been utilized for focusing, diffusing, phase shifting, or separating the two orthogonally polarized impinging EM waves in the reflection/refraction mode [24]–[28].

The major focus of this work is to design a novel AMS lens-based compact integrated antenna system to facilitate dual-polarized fan-beam patterns with independent beam-scanning ability. This type of configuration is achieved here with the help of a source antenna [differentially fed microstrip patch antenna (MPA)], a polarization rotator (PR), two actuators, and the newly designed transmission-type AMS lens. The source antenna in the present situation is realized using a MPA along with a differential feed arrangement. Due to this kind of arrangement, the source antenna can generate spherical EM waves with low cross-polar radiation, which are basically suitable for effectively illuminating the AMS lens in order to obtain fan-beam pattern with satisfactory radiation characteristics. The proposed source antenna is novel in terms of its specific design, where both the radiating aperture and the feed network (comprising a hybrid coupler and metallic strips) are sharing a common ground plane. The PR in the proposed configuration comprises two identical metallic patterned layers, and for controlling the relative orientation of these metallic layers, a passive mechanical system (designated as the actuator-1) is used here. This PR can directly process the incoming spherical EM waves as it is placed in the near field of the source antenna. The linearly polarized EM waves originating from the source antenna may pass through the PR either with the same or 90° rotated polarization depending on whether the two metallic layers of the PR are parallel or orthogonally oriented to each other. Therefore, with the help of actuator-1, the antenna subsystem (source antenna and PR) can generate two orthogonally polarized EM waves which are separately used to illuminate the aperture of the newly designed AMS lens. The planar AMS lens proposed here is quite novel as it is the first configuration of this type, comprising two individual cylindrical MS (CMS) lenses, CMS_Y and CMS_X. The phase distribution across the aperture of both CMS_Y and CMS_X lenses is cylindrical in nature, oriented along the Y- and X-directions, respectively. In the design process of AMS lens, first the basic design parameters of the CMS lens are analytically obtained from the basic theory of optics. After this, both the designed CMS lenses (CMS_Y and CMS_X) are integrated in order to obtain a single AMS lens structure. Due to this kind of integration, a unique phase profile of the AMS lens is obtained which facilitates phase correction for both types of orthogonally polarized impinging spherical EM waves (originating from the antenna subsystem) along the direction of their respective polarization only. As a result, two independent fan-beam-like radiation patterns with narrow beamwidth along the direction of their polarization and a wider beamwidth along the orthogonal direction are obtained. Now, in order to effectively scan the 2-D space, with the help of one passive mechanical system (actuator- 2), the AMS lens is translated by a distance of 60 mm along the direction of polarization of EM waves (where beamwidth is comparatively less) resulting into the beam steering in the elevation plane with the total scanning range of 60°.

To summarize, in the proposed configuration, the polarization rotation capability of the PR (aperture length: $L_{PR} = 1.925\lambda_0$) in addition to the polarization-dependent phase correction ability of the proposed AMS lens (aperture length: $L_A = 3.85\lambda_0$) are utilized by placing them at a height of $0.35\lambda_0$ and $0.77\lambda_0$ from the source antenna, respectively. The overall height of the proposed configuration (including a source antenna, a PR, and an AMS lens structure) is around 28.92 mm (λ_0), which reveals its compactness. Moreover, the designed PR and the AMS lens in the proposed configuration are quite thin planar structures with the individual thickness of only $0.07\lambda_0$ and $0.165\lambda_0$, respectively. To the best of authors' knowledge, this type of AMS-based multifunction integrated antenna system with a compact configuration has not been earlier proposed in the literature.

II. Operating Principle and Design Guidelines

In this section, the operating principle, the basic design guidelines, and the simulation method of the proposed configuration are elaborated. The proposed planar AMS lens is basically a combination of two identical CMS lenses, CMS_Y and CMS_X, which are oriented along the orthogonal directions. Since the design guideline and the corresponding beam-scanning principle for both the CMS lenses are the same, only a single CMS lens (CMS_Y) is elaborated here.

A. Design Guideline of the Cylindrical MS (CMS_Y) Lens

In the proposed configuration, the source antenna is linearly polarized along the Y-direction and generates EM waves with the spherical wavefront, as shown in Fig. 1(a). Here, the Y-component of the electric field (E_Y) dominates over other electric field components that are E_X and E_Z. To obtain a fan-beam-like pattern, these spherical EM waves are incident on a specially designed CMS lens (CMS_Y) by placing it at a focal distance F from the aperture of the source antenna. The cylindrical phase profile (ϕ_i, $i = 1$ to n) of CMS_Y lens along the Y-direction is obtained here by discretizing it with $2n$ number of unit cells (UCs), denoting by UC_i ($i = 1$ to n). The aperture dimension of this lens is $L_A \times L_A$, whereas the lateral dimension of each UC_i is $L_{UA} \times L_{UA}$. In this case, these UCs are symmetrically oriented from the center of the CMS_Y lens along the Y-direction, as depicted in Fig. 1(a). Here, the UCs placed in the middle of the CMS_Y lens introduce maximum phase delay to the impinging EM waves, whereas

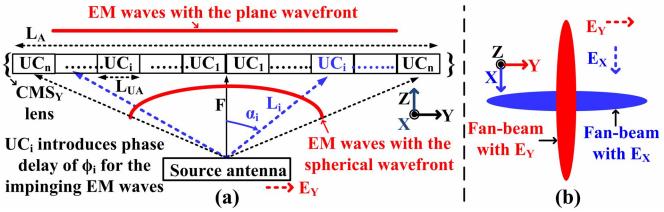

Fig. 1. (a) Phase correction of E_Y of spherical EM waves along the Y-direction by using CMS_Y lens. (b) Two orthogonally oriented fan-beam patterns with the orthogonal polarizations.

this phase delay gradually decays as one moves away from the center along the $+Y$- and $-Y$-directions. Due to this type of cylindrical phase distribution, the CMS_Y lens provides phase correction for the Y-polarized impinging spherical EM waves along the Y-direction only resulting into the fan-beam-like radiation pattern with the narrow beamwidth along the same direction (Y-direction).

The spherical EM waves originating from the source antenna are impinged on the UC_i of the planar lens by traveling a distance of L_i. This distance (L_i) is traveled by the EM waves along a path, making an angle of α_i from the normal direction (Z-direction). Here, the unit cells UC_i ($i = 1$ to n) of the discretized CMS_Y lens are introducing progressive transmission phase delay of ϕ_i ($i = 1$ to n) to the impinging Y-polarized spherical EM waves. Due to which the phase of these spherical EM waves are corrected along the same Y-direction. In order to obtain plane EM waves (along Y-direction) at the output of CMS_Y lens while illuminating through Y-polarized (E_Y) spherical EM waves, the different transmission phase delay ϕ_i required for each UC_i of CMS_Y lens can be calculated using the following relation:

$$kL_i + \phi_i = \text{constant}(i = 1, 2 \ldots n) \tag{1}$$

where $k(= 2\pi/\lambda)$ is a wave propagation constant in the free space. Here, distance L_i can easily be calculated using basic trigonometry, as given below

$$L_i = F/Cos(\alpha_i), \alpha_i = \tan^{-1}\{\{L_{UA} \times (i - 0.5)\}/F\} \tag{2}$$

where

$$L_A = 2n \times L_{UA}. \tag{3}$$

Therefore, using the given values of focal distance F, the CMS aperture dimension L_A, and the number of UCs $2n$, the transmission phase delay ϕ_i required by each UC (UC_i) can easily be determined. This 1-D phase correction actually facilitates a fan-beam-like radiation pattern with a narrow beamwidth along the direction of polarization of EM waves (Y-direction in this case) and a wide beamwidth along the orthogonal direction, where the cross-polar component of the corresponding EM waves is oriented.

B. Fan-Beam Scanning

It is observed that the system with this kind of fan-beam pattern can easily detect any object located in the direction of its wide beamwidth. However, sometimes detection may be quite challenging if the object is placed along the orthogonal direction, where beamwidth of the corresponding fan-beam is somewhat less. Therefore, in order to effectively scan 2-D space, this fan-beam is now being steered along the direction of its polarization, where the beamwidth is comparatively less. This 1-D beam scanning in the elevation plane (the YZ plane) is obtained here by translation of the CMS_Y lens along the direction of polarization (which is Y-direction in this case) of fan-beam. This translation of the lens actually introduces a linear phase slope along the direction of its movement, resulting into the beam tilts in the YZ plane by an angle of θ_Y from the normal direction. From simple array theory, the direction of the main beam (θ_Y) can be estimated as

$$\theta_Y = \sin^{-1}\{\Delta\gamma_Y/(k \times L_{UA})\}. \tag{4}$$

Here, $\Delta\gamma_Y$ a relative phase difference between the feed signals of the consecutive UCs of the lens is actually introduced by the movement of the lens. From the above relation, it is found that the continuous translation of the lens provides gradual variation in $\Delta\gamma_Y$, resulting into the fan-beam scanning (varying θ_Y) along the direction of the lens movement.

C. Source Antenna, PR, and AMS Lens

From the above discussion, it can be observed that the configuration of source antenna and CMS_Y lens can facilitate both the generation and the 1-D scanning of the Y-polarized fan-beam pattern. In order to enhance the capability of the system in terms of polarization and beam scanning, in lieu of using simple CMS_Y lens, a novel AMS-based lens structure is utilized here. This AMS lens is basically a combination of two orthogonally oriented CMS lenses that are CMS_Y (oriented along the Y-direction) and CMS_X (oriented along the X-direction), which facilitate two orthogonal cylindrical phase profiles using a single lens structure. Due to this novel phase profile, the AMS lens corrects the phase of Y- and X-polarized spherical EM waves along the Y- and X-directions, respectively. The value of transmission phase delays (ϕ_i) introduced by UC_i of the AMS lens is maximum at the center of its aperture and it is gradually decaying in the Y- and X-directions for the Y-polarized (E_Y) and X-polarized (E_X) impinging spherical EM waves, respectively. Hence, this AMS lens can facilitate two individual fan-beam-like radiation patterns corresponding to two orthogonally polarized impinging EM waves, as also shown in Fig. 1(b). The beamwidth of these fan-beams are narrow in the direction of their polarization and wide in the orthogonal directions, where corresponding cross-polar component of the electric field is oriented. In order to scan the 2-D space more effectively, these orthogonally polarized fan-beams are individually steered in the direction of their polarization by in-plane translation of the AMS lens, as already discussed in Section II-B.

It is important to note that due to the special design of the AMS lens (comprising CMS_Y and CMS_X lenses), apart from correcting the phase of the copolar radiation, it certainly affects the phase of cross-polar radiation, which may degrade the overall radiation performance of the proposed configuration. In order to overcome this problem, the AMS lens in the present situation should be illuminated through the spherical EM waves with the low cross-polar radiation component. By reducing the cross-polar radiation level of the EM waves

by the source antenna itself, the AMS lens would produce fan-beam radiation patterns more precisely. Therefore, for the polarization purity (low cross-polar radiation), a differentially fed linearly polarized (in Y-direction) MPA is used here as a source element. Moreover, in order to illuminate the AMS lens with two orthogonally polarized spherical EM waves individually, a PR is placed in the cavity formed between the source antenna and the AMS lens. This PR either maintains the polarization (E_Y) of the impinging spherical EM waves originating from the source antenna or rotates it by 90° to achieve spherical EM waves with the orthogonal polarization E_X. These two independently obtained orthogonally polarized spherical EM waves at the output of the PR are finally used to excite the AMS lens individually. Here, it is to be mentioned that the AMS lens can produce either Y-polarized (E_Y) fan-beam (narrow beamwidth in the Y-direction) or X-polarized (E_X) fan-beam (narrow beamwidth in the X-direction), depending upon the polarization of the impinging spherical EM waves obtained through the antenna subsystem (source antenna and PR). It basically means that these fan-beam patterns [shown in Fig. 1(b)] are not obtained simultaneously.

D. Simulation Method

First, each element of the proposed configuration such as the hybrid coupler, the capacitively coupled MPA, the PR, and the AMS lens are individually designed using the CST Microwave Studio software. The MPA along with two metallic strips are simulated here by exciting the structure using two out of phase signals with equal amplitudes. After that, a hybrid coupler operating in a wide frequency band (including frequency band of the MPA) is designed and coupled to the input ports of the antenna using two metallic vias. This source antenna (MPA and feed network) is now used as a source of the spherical EM waves in the proposed configuration. In the next step, the UCs corresponding to PR and AMS lens are individually simulated using a two-port simulation model, as discussed in Section III. After this two-port simulation, the response of each of the aforementioned UCs is individually used to design the PR and the AMS lens independently. These designed PR and the AMS lens are placed at a certain height (in the near field of source antenna) from the aperture of the source antenna. Afterward, the simulation is carried out to slightly optimize the parameters (height and other dimensions) of the antenna subsystem (source antenna and PR) and the proposed configuration (source antenna, PR, and AMS lens) in order to obtain better beam shapes. Finally for beam scanning, the simulations are carried out for various orientations of the AMS lens placed above the antenna subsystem (source antenna and PR).

III. Performance of the Individual Elements

In the proposed configuration, the source antenna (MPA and feed network), the PR, and the AMS lens are placed in a specific arrangement, as depicted in Fig. 2(a). The design methodology and results of each element including its individual performance are discussed in this section.

A. Feed Network

In order to excite the MPA with differential signals, a feed network comprising a microstrip line, a wideband hybrid

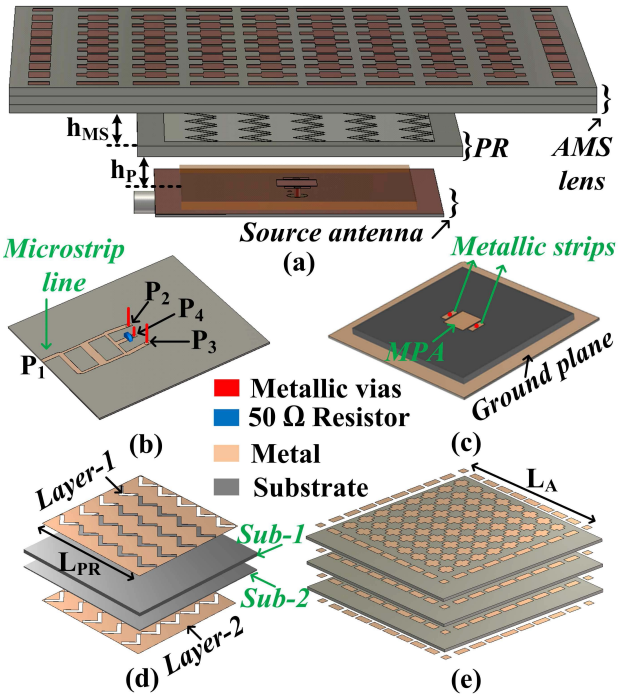

Fig. 2. Geometry of the proposed configuration. (a) Proposed structure (h_P = 10 mm, h_{MS} = 10 mm). (b) Part of the feed network placed at the bottom side of the ground plane. (c) MPA with metallic strips placed at the top side of the ground plane. (d) Geometry of the PR with two metallic layers (aperture length: L_{PR} = 55 mm). (e) Geometry of the AMS lens with four metallic layers (aperture length: L_A = 110 mm).

coupler, two metallic vias, and two metallic strips is used here [shown in Fig. 2(b) and (c)]. A hybrid coupler is a four-port (P_1 to P_4) device, where the input port (P_1) is connected to the microstrip line. The signal is fed in the microstrip line through input port (P_1) of the hybrid coupler. In the ideal case, two out of phase signals with equal amplitudes are obtained at the output ports that are Port 2 (P_2) and Port 3 (P_3) of the hybrid coupler. These ports (P_2, P_3) are connected with the metallic strips [which are coplanar to the MPA, as shown in Fig. 2(c)] using two metallic vias, passing through the substrate and the circular slots etched out in the ground plane. Here, in order to provide perfect isolation between the ground plane and these metallic vias, two circular slots are etched on the ground plane. Finally, differential signals obtained at the metallic strips are capacitively coupled to the MPA. These differential signals mainly ensure here lower cross-polar radiation of the MPA [29], [30]. In the hybrid coupler, small amount of the signal is also coupled from P_1 to the isolated port that is Port 4 (P_4). Hence, P_4 is terminated here with a 50 Ω chip resistor in order to minimize the reflected signals from this port (P_4). The other end of 50 Ω resistor is connected to the ground plane using one metallic via, as shown in Fig. 2(b). It is to be noted here that both the hybrid coupler and the MPA are sharing a common ground plane, which is placed in-between of them.

The hybrid coupler used in this configuration is a wideband two-section coupler printed on a Taconic TLY-5A ($\epsilon_r = 2.17$, thickness = 0.51 mm) substrate, as shown in Fig. 3. The lengths and impedances of different lines are taken from [31], which are further calculated and optimized to operate the hybrid coupler in a desired frequency band. The S-parameter

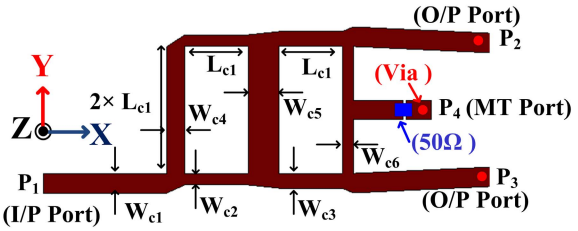

Fig. 3. Top view of the hybrid coupler with parameters ($W_{c1} = 1.58$, $W_{c2} = 0.937$, $W_{c3} = 1.2$, $W_{c4} = 1.455$, $W_{c5} = 2.49$, $W_{c6} = 0.9$, and $L_{c1} = 5.5$) (all lengths in millimeters).

response of the stand-alone hybrid coupler in terms of amplitude and phase is plotted in Fig. 4(a). At the operating frequency of 10.5 GHz, matching characteristics (magnitudes of S_{11}, S_{22}, and S_{33}) for all the ports of the hybrid coupler are better than -20 dB, whereas isolation (S_{32}, between output ports P_2 and P_3) is better than -17.0 dB. It is also found that the coupling from P_1 to P_2 (S_{21}) and P_1 to P_3 (S_{31}) are almost identical and approximately equal to -3.0 dB. The differential behavior of the coupler can easily be observed here by the parameter $\angle S_{21} - \angle S_{31}$, which is approximately equal to 180°. This parameter basically shows the phase difference between the signals appearing at the O/P ports (P_2 and P_3), while a hybrid coupler is fed through port P_1. Hence, the designed coupler is operated in a wideband centered at the frequency of 10.5 GHz and providing the desired differential signals in order to feed the MPA.

B. Capacitively Coupled MPA

A differentially driven MPA with the lower cross-polar radiation is used here to excite the AMS lens. The antenna can be differentially driven by feeding through two out of phase signals with the equal amplitudes. As mentioned in Section III-A, these kind of feed signals can easily be extracted from the O/P ports (P_2 and P_3) of the hybrid coupler. Here, distance between feed ports (or O/P ports, P_2 and P_3 of the hybrid coupler) of antenna plays a vital role for achieving the resonance, which must be greater than $0.1\lambda_0$, as reported in [29]. Since these feed ports are incorporated along the resonating length of the MPA, this distance would also be lesser than $0.5\ \lambda_g$. In the operating frequency band centered at 10.5 GHz, the physical length of the resonating arm of the MPA becomes very less (only in few millimeters). Therefore, with this design constraint (minimum separation: $0.1\lambda_0$ and maximum separation: $0.5\lambda_g$), sometimes fabrication of the MPA with these two feed ports becomes quite challenging. Hence, in lieu of a dual-feed simple MPA, a capacitively coupled MPA is used here, where location of the feed ports becomes quite far from each other. Moreover, limitations of the maximum separation of $0.5\lambda_g$ is also get abolished. The detail investigation of a capacitively coupled single port MPA is already explored in [32], hence omitted here for brevity. Therefore, in the configuration of source antenna, the MPA is capacitively coupled with the two metallic strips, which are connected with the O/P ports of the hybrid coupler using two metallic vias.

The top view of the linearly polarized (in the Y-direction) MPA with two metallic strips and their corresponding design dimensions are given in Fig. 4(b). This antenna is printed on the Taconic TLY-5A ($\epsilon_r = 2.17$, thickness $= 1.58$ mm)

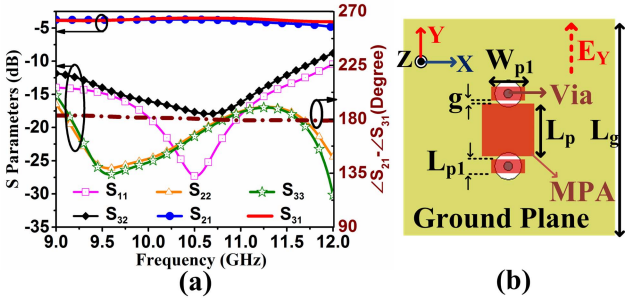

Fig. 4. (a) S-parameter response of the hybrid coupler. (b) Top view of the MPA with the metallic strips ($L_p = 7.8$, $L_{p1} = 2.0$, $g = 0.5$, $W_{p1} = 5.0$, and $L_g = 55.0$) (all lengths in millimeters).

substrate. Here, individual centers of each metallic strips are separated by a distance of 10.8 mm (L_p+2g + L_{p1}) and connecting with the O/P ports (P_2 and P_3) of the hybrid coupler using two metallic vias. The source antenna is basically fed through input (I/P) port P_1 of the hybrid coupler, where the simulated and measured reflection coefficients are obtained. It is investigated that in addition to the resonating length ($L_p = 0.5\lambda_g$) of the MPA, matching characteristics of the source antenna is also influenced through two parameters that are g (separation between radiating edge of the MPA and the metallic strip) and L_{p1} (width of the metallic strip). These parameters (g and L_{p1}) basically controls the capacitive coupling between the MPA and the metallic strips, hence plays a dominant role while achieving the overall matching performance. In order to achieve adequate matching at the operating frequency of $f_0 = 10.5$ GHz, these parameters are optimized as shown in Fig. 5(a) and (b). The source antenna is designed with the finally optimized parameters of $g = 0.5$ mm and $L_{p1} = 2.0$ mm, where maximum matching is achieved, as shown in Fig. 5(c).

The simulated and measured impedance bandwidths of the finally optimized source antenna are 960 MHz (10.28–11.24 GHz) and 1200 MHz (10.4–11.6 GHz), respectively. Here, slight discrepancy between the simulated and the measured results may be due to the spacing between the substrate and the ground plane of the MPA, which was not taken into the account during the simulation process, although appeared in the final fabricated prototype. However, both the simulated and measured S-parameters are better than -15 dB at the operating frequency of $f_0 = 10.5$ GHz. The simulated and measured 2-D radiation patterns of the source antenna in the XZ plane (H-plane) and YZ plane (E-plane) are shown in Fig. 5(d). In this case, electric field components E_ϕ and E_θ are the copolarized components in the XZ and YZ planes, respectively. These results confirm that the source antenna is linearly polarized along the Y-direction and radiates in the broadside direction with the lower cross-polar radiation (cross polarization level less than -30 dB), which shows the utility of using the differential feed signals. It is to be mentioned here that the ground plane also minimizes the effect of the unwanted spurious radiation of the hybrid coupler on the radiation pattern of the MPA.

C. Polarization Rotator

In order to achieve two orthogonally polarized spherical EM waves independently, a PR is placed at a height of

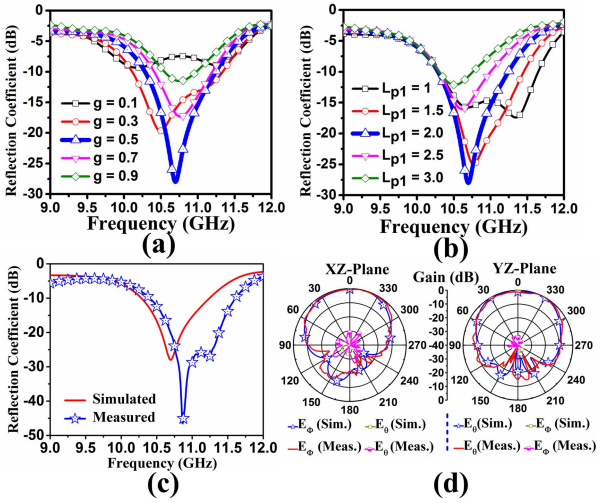

Fig. 5. Variations of reflection coefficient (S_{11}) of the source antenna with: (a) g (in millimeters). (b) L_{P1} (in millimeters). (c) Reflection coefficient of the finally optimized source antenna. (d) Radiation patterns of the source antenna (at $f_0 = 10.5$ GHz) in the two orthogonal planes.

$h_p (= 0.35\lambda_0 = 10$ mm) from the aperture of the source antenna, as depicted in Fig. 2(a). It is to be noted that the spherical EM waves originating from the source antenna are basically polarized along the Y-direction, while impinging on the bottom layer of the PR. The PR [Fig. 2(d)] comprised two identical metallic pattern layers, Layer-1 and Layer-2 printed on two dielectric substrates Sub-1 (thickness = 1.58 mm) and Sub-2 (thickness = 0.51 mm) of material Taconic TLY-5A ($\epsilon_r = 2.17$), respectively. Now, with the help of one actuator (actuator-1), Layer-1 can be independently rotated above Layer-2. In this case, Layer-2, along with the source antenna, is kept in a fixed position. For each 90° rotation of the Layer-1, the PR either preserves the polarization E_Y of the impinging EM waves or rotates it by 90° to achieve EM waves with the orthogonal polarization E_X.

The PR in the proposed configuration comprised an array of 5×5 UCs, where each UC is consisting of two identical metallic pattern layers. Here, one V-shaped slot etched out from each metallic layer is basically a combination of two orthogonal slots of dimensions $L_1/2 \times W_s$, as depicted with its design dimensions in Fig. 6. The operating frequency of the UC of PR is controlled by the resonating length (L_1) of the V-shaped slot, which must be equal to $\lambda_g/2$ [33]. The response of this UC for the Y-polarized (E_Y) impinging EM waves depends on the relative orientations of the V-shaped slots etched at the top and the bottom metallic layers, as clearly observed from Fig. 6(a) and (b). In the first case (Case-I), both V-shaped slots present at the top and the bottom layers of the UC are parallel to each other. Due to this kind of configuration, the UC of PR transmits the Y-polarized EM waves without altering its polarization, as shown in Fig. 6(a), whereas in the second case (Case-II), the top layer of the UC is rotated by an angle of 90° while keeping bottom layer in a fixed position. Although, for this new configuration, V-shaped slot present at the bottom metallic layer of UC still supports the Y-component of electric field (E_Y), this E_Y eventually gets rotated by 90° and becomes E_X after transmitting through the V-shaped slot present at the top metallic layer, as clearly observed from Fig. 6(b).

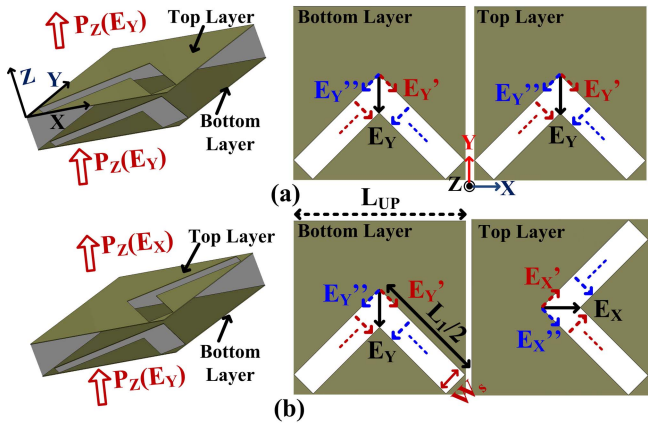

Fig. 6. Response of UC of PR in (a) Case-I and (b) Case-II (dimensions: $L_{UP} = 11$, $L_1 = 14.3$, and $W_s = 1.6$) all length in millimeters.

Hence, on the basis of the relative orientations of these aforementioned V-shaped slots present at the top and the bottom metallic layers, the PR can transmit the impinging EM waves either with the same Y-polarization (consider as a Case-I) or rotates it by 90° into the X-polarized EM waves (consider as a Case-II). In order to characterize the UC of the PR in both of the aforementioned cases (Case-I and Case-II), three parameters (T_{YY}, T_{XY}, and R_{YY}) relating the electric field components of the incident and the transmitted/reflected EM waves are defined here. Theses parameters are copolarized transmission coefficient ($T_{YY} = (|E_{tY}|/|E_{iY}|)$), cross-polarized transmission coefficient ($T_{XY} = (|E_{tX}|/|E_{iY}|)$), and copolarized reflection coefficient ($R_{YY} = (|E_{rY}|/|E_{iY}|)$). Here, E_{iY}, E_{tY}, and E_{rY} are the electric field components of the Y-polarized incident, transmitted, and reflected EM waves, respectively, whereas E_{tX} is the electric field component of the X-polarized transmitted EM waves. The variations in the aforementioned parameters with frequency is shown in Fig. 7(a). It is found that T_{YY} for Case-I and T_{XY} for Case-II are better than 0.95, whereas reflection coefficients (R_{YY}) for both cases are less than 0.1 in the operating frequency band. It is to be mentioned that this response is obtained by simulating aforementioned UC of PR in CST Microwave Studio software using a two-port simulation model, as shown in Fig. 7(b). Since this model is the same for both cases (except relative orientations of top and bottom layers), it is depicted only for Case-I. During this simulation, the plane waves are impinged on the UC from the normal direction (Z-direction). Here, UC boundary conditions are imposed in the two orthogonal planes (the YZ and XZ planes), which are also perpendicular to the direction (Z-direction) of the propagation of plane waves.

D. Anisotropic Metasurface Lens

In the proposed configuration, a novel AMS-based lens structure is designed and placed at a focal distance F from the aperture of the source antenna, as shown in Fig. 2(a). This AMS lens is basically a combination of two CMS lenses, CMS_Y and CMS_X, as portrayed in Fig. 8. The UC of CMS lens with the cross section of $L_{UA} \times L_{UA}$ is made up of four identical patch-shaped metallic pattern layers, separated by three dielectric substrates (Taconic TLY-5A, $\epsilon_r = 2.17$, thickness = 1.58 mm). It is to be mentioned here that the

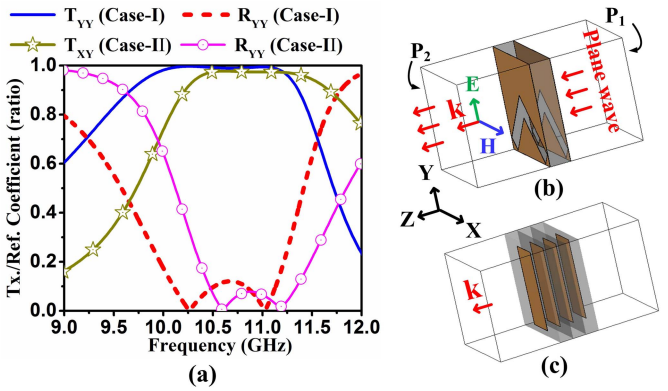

Fig. 7. (a) Simulated response of UC of PR for Y-polarized (E_{iY}) incident EM waves in two different cases (Case-I and Case-II). Two-port simulation model of UC of (b) PR for Case-I and (c) CMS lens (CMS_Y).

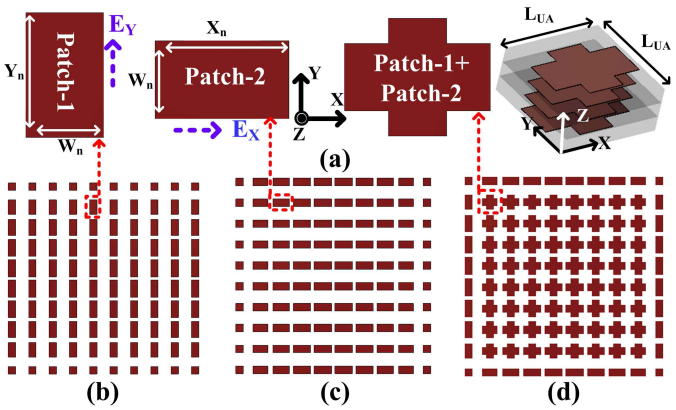

Fig. 8. Designing of the AMS lens using CMS lenses. (a) UCs of different MSs. Front view of (b) CMS_Y, (c) CMS_X, and (d) the proposed AMS lens ($L_{UA} = 11$ mm).

four metallic layer structure is chosen here to enhance the transmission phase range [27]. A single metallic layer of CMS_Y and CMS_X lenses comprised metallic patches, Patch-1 ($W_n \times Y_n$) and Patch-2 ($X_n \times W_n$), respectively. In order to obtain cylindrical phase profile of CMS_Y lens along the Y-direction, the Y-directed dimension Y_n of Patch-1 is varied in the Y-direction, as shown in Fig. 8(b). In the same way, the X-directed dimension X_n of Patch-2 is varied along the X-direction [Fig. 8(c)] for introducing cylindrical phase profile of CMS_X lens along the X-direction. Due to this kind of phase profile, CMS_Y and CMS_X lenses introduce phase correction for the Y- and X-polarized spherical EM waves along the Y- and X-directions, respectively. The front view of the finally proposed AMS lens (which is basically a combination of CMS_Y and CMS_X lenses) is shown in Fig. 8(d). The UC of AMS lens is also a four identical cross-shaped metallic patterned layer structure, where each single cross-shaped metallic pattern is basically a combination of aforementioned rectangular patches, Patch-1 and Patch-2. These two orthogonal patches are mainly responsible here for introducing two independent orthogonal cylindrical phase profiles in a single AMS lens structure, as discussed in Section II-C.

In the designing of AMS lens, first both CMS_Y and CMS_X lenses are separately designed. Afterward these lenses are combined in order to accomplish the proposed AMS lens. Although CMS_Y and CMS_X lenses are oriented along the orthogonal directions, for symmetry, the dimensions Y_n ($n =$ 1–5) of Patch-1 are kept equal to X_n of Patch-2. Therefore, design description of the CMS_Y lens is only demonstrated here for brevity. The two-port simulation of UC of the CMS_Y lens is carried out using CST Microwave studio software, as shown in Fig. 7(c). Here, this UC is illuminated through Y-polarized and X-polarized plane EM waves, independently while varying dimension Y_n of Patch-1 from 4 to 9.3 mm and keeping other dimensions ($W_n = 4$ mm) at the fixed value. The transmission response (in terms of phase and magnitude) of this type of UC with different values of Y_n is depicted in Fig. 9(a). In this figure, t_{XX}/ϕ_{XX} and t_{YY}/ϕ_{YY} are denoting transmission magnitude/transmission phase of the aforementioned UC, while illuminating through X- and Y-polarized EM waves, respectively. For different values of Y_n ($Y_n = 4$ to 9.3), the values of t_{XX} and t_{YY} are found to be better than 0.85. Moreover, in terms of phase, ϕ_{XX} is almost constant to $-105°$, whereas ϕ_{YY} is gradually varying. It is interesting to observe that Y_n, the Y-directed dimension of Patch-1, significantly affects the phase of Y-polarized incident EM waves, whereas it merely affects the phase of X-polarized EM waves. Hence, an array of these UCs with different values of Y_n can be used for correcting the phase of Y-polarized incident spherical EM waves along the Y-direction. In the same way, the CMS_X lens is designed by varying the X-directed dimension X_n of Patch-2. This designed CMS_X lens corrects the phase of X-polarized incident spherical EM waves along the X-direction, accordingly.

In order to design the CMS_Y lens from the basic principle illustrated in Section II, the transmission response of UC [Fig. 9(a)] is utilized here. The CMS_Y lens can be designed with the given values of Focal distance F, aperture dimension L_A, and number of UCs $2n$. In order to correct the phase of spherical EM waves using a compact configuration, these parameters are chosen here such that: $F/L_A = 1/5$ where $F = 0.77\lambda_0$ (22 mm) and $L_A = 3.85\lambda_0$ (110 mm). Although, different sets of focal distance (F) and aperture dimension (L_A) can also be chosen. This CMS_Y lens is discretized by $2n$ ($= 10$) number of UCs, where dimension of each UC is obtained as $L_{UA} = 0.385\lambda_0$ (11 mm), as shown in Fig. 8. These UCs are symmetrically oriented ($n =$ 1–5) from the center of the aperture of the CMS_Y lens toward positive and negative Y-axis. Now, with the aforementioned values of $F = 0.77\lambda_0$, $L_A = 3.85\lambda_0$, and $2n = 10$, various parameters (listed in Table I) of the designed CMS_Y lens can be calculated using Eqs. (1)–(3), expressed in Section II. After designing CMS_Y lens, parameters of the CMS_X lens are also obtained while considering Y_n of Patch-1 $= X_n$ of Patch-2 (where $n =$ 1–5). Finally, the proposed AMS lens is designed by combining both CMS lenses, CMS_Y and CMS_X, with the given values of X_n and Y_n, listed in Table I. Here, it is to be clarified that the modulation of the broadside radiation pattern originating from the antenna subsystem into fan-beam pattern basically depends on the relative phase distribution (not absolute) of the UCs. After calculation, dimensions Y_n/X_n of UCs are slightly optimized in order to obtain better beam shape.

The front view of the finally designed AMS lens is shown in Fig. 9(b). It can easily be observed from this figure that

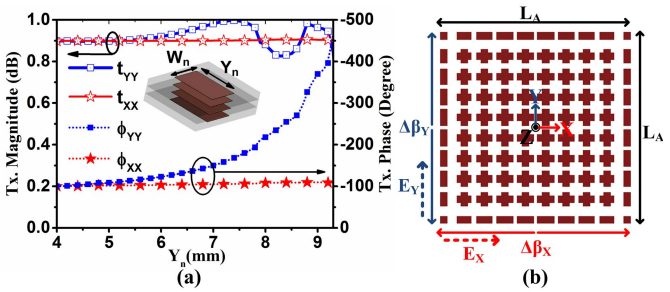

Fig. 9. (a) Transmission response of UC of CMS_Y lens. (b) Front view of AMS lens with its phase response ($\Delta\beta_Y/\Delta\beta_X$) corresponding to two orthogonally polarized impinging EM waves ($L_A = 110$ mm).

the dimension Y_n of Patch-1 is gradually decaying as one moves away from the center of the aperture of the AMS lens toward both +Y and −Y directions. In the same way, the dimension X_n of Patch-2 is also gradually decaying from the center of the aperture of the AMS lens toward both +X and −X directions. This gradual decay in the dimension of Y_n and X_n actually facilitates a linear phase correction for Y- and X-polarized impinging spherical EM waves along the Y- and X-directions, respectively. Due to this unique phase profile of the AMS lens, impinging spherical EM waves polarized along the Y (E_Y) and X-directions (E_X) feel the phase correction of $\Delta\beta_Y$ and $\Delta\beta_X$ along the Y- and X-directions, respectively. This results into the fan-beam-like radiation patterns with the narrow beamwidth along the direction of phase correction. It is to be mentioned here that the other dimensions ($W_n = 4$ mm, $n = 1$–5) of both Patches (Patch-1 and Patch-2) of UCs are kept constant in the designing of the AMS lens. Therefore, the proposed planar AMS lens can provide two independent fan-beam-like radiation patterns with the narrow beamwidth in either the Y- or X-direction depending upon the polarization of the impinging spherical EM waves. It is also found that, apart from rotating polarization axis by 90°, the PR (discussed in Section III-C) may also slightly modify the spherical phase distribution of the EM waves originating from the source antenna. Therefore, the AMS lens in the present situation is illuminated through the EM waves which are almost (not exact) spherical in nature and, hence, at the output of the AMS lens a reasonably fan-beam-like radiation patterns are obtained.

IV. Design of the Integrated Systems

The major performance including the results of the stand-alone elements of the proposed configuration such as hybrid coupler, source antenna, UC of PR, and UC of AMS lens have already been discussed in Section III. In this section, outcomes of the antenna subsystem (source antenna and PR) and the proposed complete integrated antenna system (source antenna, PR, and AMS lens) are validated through both simulation and measurement. It is to be mentioned here that in the first case (Case-I), the polarization (E_Y) of the spherical EM waves originating from the source antenna remains preserved after passing through the PR and, hence, the AMS leans gets illuminated through the Y-polarized EM waves. Contrary to this, in the second case (Case-II), the PR rotates the polarization (E_Y) of the spherical EM waves by 90° and, hence, X-polarized (E_X) EM waves are obtained at the output of the PR, which are finally used to illuminate the AMS lens. This terminology (Case-I and Case-II) is adopted throughout this paper.

TABLE I
Different Design Parameters of the AMS Lens

UC_i	α_i	L_i (mm)	kL_i	norm. ϕ_i	Y_n/X_n
UC_1	14.03°	22.67	285.64°	-397.28°	9.3
UC_2	36.86°	27.49	346.37°	-336.55°	9.1
UC_3	51.34°	35.21	443.64°	-239.28°	8.7
UC_4	60.25°	44.33	558.55°	-124.37°	7.8
UC_5	66.03°	54.15	682.92°	0.0°	4.0

A. Radiation Patterns

The radiation patterns of the antenna subsystem (source antenna and PR) and the proposed configuration (source antenna, PR, and AMS lens) are discussed in this section.

1) Antenna Subsystem (Source Antenna and PR): The 2-D simulated and measured radiation patterns of the antenna subsystem (source antenna and PR) in Case-I and Case-II are shown in Fig. 10(a) and (b), respectively. It can be observed from Fig. 10(a) that E_ϕ and E_θ are the copolarized radiation components in the XZ and YZ planes, respectively, whereas in Fig. 10(b), these electric field components are getting reversed that is E_θ and E_ϕ become the copolarized radiation components in the XZ and YZ planes, respectively. The aforementioned results confirm the polarization rotation capability of the PR by changing the relative orientations of Layer-1 above Layer-2. Here, it can be noted that the measured and simulated radiation patterns are almost identical; however, a slight tilt in the direction of the main beam can be observed in the measured radiation pattern of Fig. 10(b). In this case, during the measurement process, the antenna subsystem was probably not properly mounted in the direction of the main beam of horn antenna, which may cause into the slight tilt of measured radiation patterns. It is also observed that apart from controlling the polarization state of the impinging EM waves, the shape of the radiation beam originating from the source antenna also gets modified due to the presence of the PR. This reshaping of beam shape actually reflects slight modification in the spherical nature of the EM waves, which are finally used to illuminate the AMS lens.

2) Proposed Configuration (Source Antenna, PR, and AMS Lens): The 2-D simulated and measured fan-beam-type radiation patterns obtained from the proposed configuration in two different cases are shown in Fig. 11. The half power beamwidth (HPBW) of these fan-beam patterns depends on the polarization and the phase distribution across the wavefront of the corresponding impinging EM waves. In Case-I, a fan-beam-type radiation pattern with narrow beamwidth (HPBW: 22.0°) in the YZ plane and wider beamwidth (HPBW: 45.0°) in the XZ plane is obtained, as depicted in Fig. 11(a). Contrary to this, a fan-beam-type radiation pattern with narrow beamwidth (HPBW: 27.0°) in the XZ plane and wider beamwidth (HPBW: 48.0°) in the YZ plane is obtained, as shown in Fig. 11(b).

B. Beam Scanning

In order to achieve 1-D beam scanning, the AMS lens is translated along the direction of polarization of fan-beam

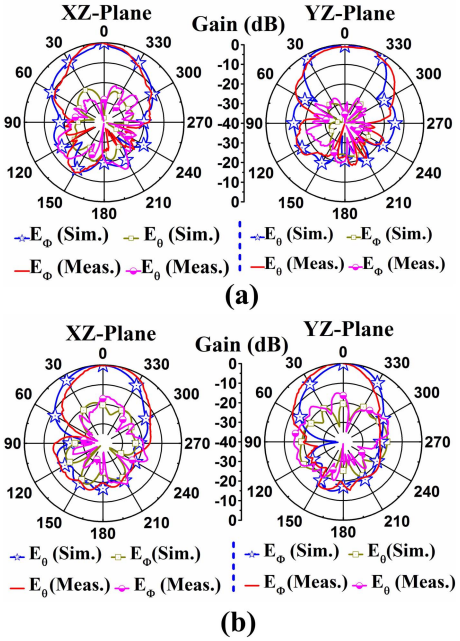

Fig. 10. 2-D radiation patterns (at $f_0 = 10.5$ GHz) of the antenna subsystem (source antenna and PR) in (a) Case-I and (b) Case-II.

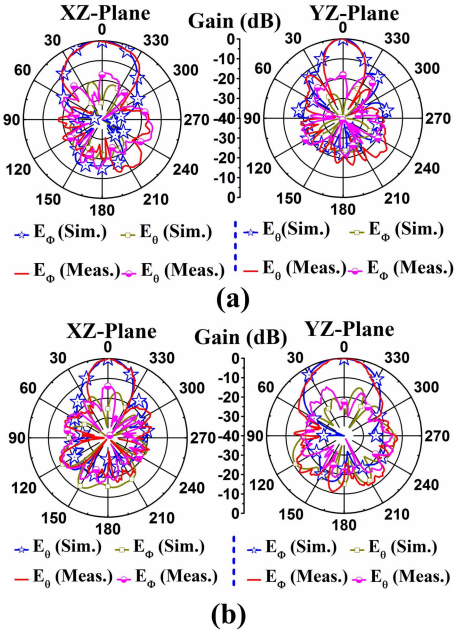

Fig. 11. 2-D radiation patterns (at $f_0 = 10.5$ GHz) of the proposed configuration in (a) Case-I and (b) Case-II.

patterns, as discussed in Section II-B. It is interesting to found that this translation (in millimeters) of AMS lens steers the direction (θ_Y or θ_X) of the main beam in the elevation plane with the resolution of 1°/mm. As a proof of concept, the AMS lens is translated along the direction of polarization of fan-beams by a total distance of 30 mm in the steps of 10 mm ($L_{AY} = 10$ mm in Case-I and $L_{AX} = 10$ mm in Case-II). This displacement of AMS lens from $L_{AY} = 0$ mm to $L_{AY} = +30$ mm in Case-I steers the direction of the main beam in the YZ plane from $\theta_Y = 0°$ to $\theta_Y = +30°$, as depicted in Fig. 12(a)–(d). In the same way, translation of the AMS lens from $L_{AX} = 0$ mm to $L_{AX} = +30$ mm in Case-II steers the direction of the main beam in the XZ plane from $\theta_X = 0°$ to $\theta_X = +30°$, as depicted in Fig. 12(e)–(h). It can be noted here that translation of the AMS lens by total distance of 30 mm in one direction facilitates beam steering with the total scanning range of 30°. Moreover, due to the symmetric configuration, the in-plane movement of the AMS lens by 30 mm in the $-Y$-direction in Case-I and $-X$-direction in Case-II will also introduce beam steering upto $\theta_Y = -30°$ and $\theta_X = -30°$ from the normal direction in the YZ and XZ planes, respectively. Therefore, the proposed configuration facilitates total beam-scanning range of 60° by total translation of the AMS lens by 60 mm. For validation of the simulated results, measurements are also carried out for all the aforementioned positions of the AMS lens above the antenna subsystem (source antenna and PR) in both cases (Case-I and Case-II). The 2-D simulated and measured results are shown in Fig. 13. It is to be noted that these results are plotted in the vertical planes (the YZ plane in Case-I and the XZ plane in Case-II), where beam steering is obtained.

Translation of the AMS lens by more than 60 mm in the present situation can further enhance the beam-scanning range; however, due to the diffraction from the edges of the AMS lens, sidelobe level (SLL) may also be deteriorated. In order to suppress these SLL while achieving large beam-scanning range, the AMS lens with comparatively large aperture size ($L_A > 3.85\lambda_0$) can be placed at somewhat large focal distance ($F > 0.77\lambda_0$) from the aperture of source antenna. In that situation, a new phase adjusting range will be incorporated throughout the aperture of the AMS lens by discretizing it by more than ten number ($2n > 10$) of UC elements. This configuration with the same value of F/L_A would increase the total scanning range beyond 60° by translating the AMS lens by more than 60 mm. Here, although beam-scanning range can be improved, the overall volume of the proposed configuration will also significantly increase, which is undesirable in this work. Since the objective of this work is to achieve independent beam scanning of dual-polarized fan-beam radiation patterns while utilizing the compact configuration, the AMS lens is discretized here by only ten number of elements ($2n = 10$) by considering comparatively less aperture size ($L_A = 3.85\lambda_0$) of the AMS lens. Therefore, in order to fulfill the objective of this work, a tradeoff is to be made between the aperture size of AMS lens and the total scanning range. As our main aim in this work is to design multifunctional integrated antenna system using a compact configuration, here a somewhat lower value of the beam-scanning range can be tolerated.

Apart from this, in these kind of configurations, beam scanning can be obtained by mechanically moving either the source antenna or the MS lens. However, in the first approach, a heavy front-end is needed to be placed on the antenna-moving platform which basically requires a bulky movable system and, hence, overall volume of the structure would be increased [34]. For the movement of the source antenna, a rotatory joint can also be employed between the front-end and the source antenna, which may lead to impedance mismatching at the input port of the antenna results into unreliable operation. The

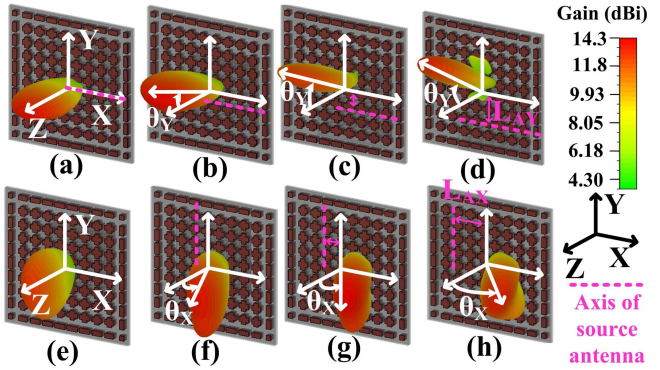

Fig. 12. Simulated 3-D radiation patterns (at $f_0 = 10.5$ GHz) for different orientations (L_{AY}/L_{AX}) of the AMS lens. Case-I: (a) $L_{AY} = 0$, (b) $L_{AY} = 10$, (c) $L_{AY} = 20$, and (d) $L_{AY} = 30$. Case-II: (e) $L_{AX} = 0$, (f) $L_{AX} = 10$, (g) $L_{AX} = 20$, and (h) $L_{AX} = 30$ (all lengths in millimeters).

objective of this work is to design an integrated antenna system for those specific applications where compact and reliable configuration is required. Hence, in the proposed configuration, source antenna is intentionally chosen to be stationary in order to avoid bulky movable system and fault-prone rotary joints, while maintaining the overall compactness of the proposed configuration. Therefore, the proposed configuration utilizes two actuators (actuator-1 for PR and actuator-2 for AMS lens) to facilitate independent beam scanning of dual-polarized fan-beam radiation patterns. It is to be mentioned that one additional actuator is tolerated here for facilitating multifunction fan-beam antenna system.

C. Matching Characteristics, Gain, and Simulated Radiation Efficiency

The simulated and measured reflection coefficients of the proposed configuration in both cases (Case-I and Case-II) are shown in Fig. 14. Although the source antenna is designed to resonate in the frequency band centered at 10.5 GHz [Fig. 5(c)], the matching characteristics of the overall configuration are somewhat modified. This modification may be due to the internal reflections of the EM waves inside the cavities formed between the source antenna and the PR and between the PR and the AMS lens. It is observed that overall matching performance at the input port of the source antenna is slightly modified due to these internal reflections, although an adequate matching is still achieved for both cases at the design frequency of 10.5 GHz. In the proposed configuration, variation in the simulated gain and measured gain with frequency are also shown in Fig. 14. In the overlapping frequency range (−10 dB impedance bandwidth starting from 10.3 to 11.3 GHz) for both cases, the measured gain varies in the range of 10.0–14.0 dBi. In the proposed configuration, since AMS lens corrects the phase of the impinging spherical EM waves along a single direction only as compared to pencil-beam pattern, somewhat lower values of the gain are expected, as also validated from these results.

In the operating frequency range (10.3–11.3 GHz), the simulated radiation efficiency of the proposed configuration for different orientations of the AMS lens that are L_{AY} in Case-I and L_{AX} in Case-II are shown in Fig. 15(a) and (b), respectively. For all the situations, these radiation efficiencies

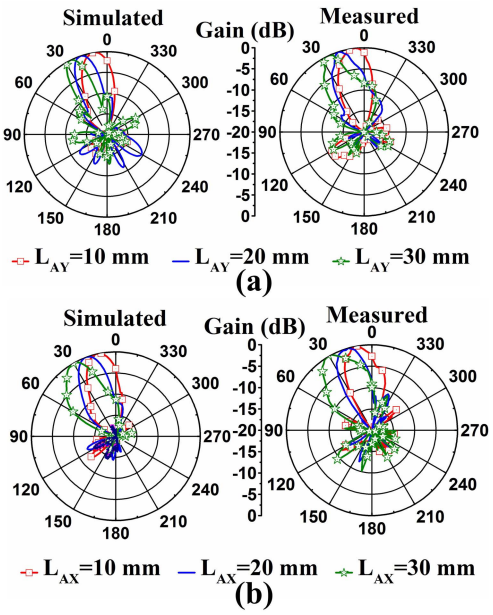

Fig. 13. Beam scanning (at $f_0 = 10.5$ GHz) of (a) Y-polarized fan-beam in the YZ plane ($\phi = 90°$) in Case-I and (b) X-polarized fan-beam in the XZ plane ($\phi = 0°$) in Case-II.

are directly obtained through simulation using a full-wave EM solver, CST Microwave Studio. Since both PR and AMS lens are designed with high transmission characteristics, these elements would not significantly affect the overall radiation efficiency of the entire system. Therefore, the overall efficiency remains high although multilayered structure is utilized in the proposed configuration. In the first stage, when PR is placed above the source antenna, the approximate radiation efficiency of 0.95 is obtained. The efficiency in the order of 0.9 is achieved, when AMS lens is placed above the antenna subsystem (source antenna and PR). Therefore, the overall efficiencies in both cases (Case-I and Case-II) are almost the same and better than 0.9 in the operating frequency range. The performance of the proposed configuration in terms of efficiency is also maintained during the beam-scanning process.

D. Fabricated Prototypes and Measurement Setup

The fabricated prototypes of the proposed configuration with its different elements are shown in Fig. 16(a)–(f). The back and front views of the source antenna are shown in Fig. 16(a) and (b), respectively. The ground plane placed between the hybrid coupler and the MPA is also shown in Fig. 16(b). Since the PR comprised two identical metallic layers, only one of them is shown in Fig. 16(c). In the same way, one metallic layer of the AMS lens (basically comprising four identical metallic layers) is depicted in Fig. 16(d). The antenna subsystem (source antenna and PR), where PR is placed at a height $h_p = 10$ mm from the aperture of the source antenna, is shown in Fig. 16(e). Finally, the overall configuration, where AMS lens is placed at an approximate height of F = 22 mm from the aperture of source antenna (or at a height of $h_{MS} = 10$ mm from the aperture of PR), is depicted in Fig. 16(f).

The radiation pattern measurement setup of the proposed configuration in the anechoic chamber is shown in Fig. 16(g).

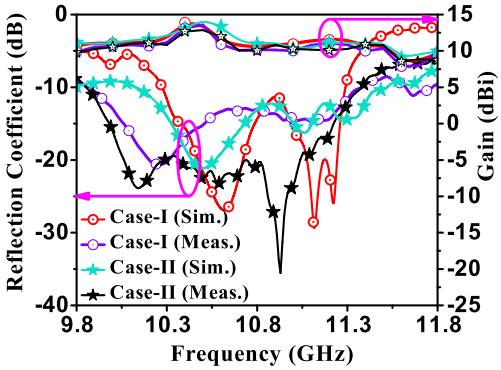

Fig. 14. Matching characteristics and gain of the proposed configuration in both cases (Case-I and Case-II).

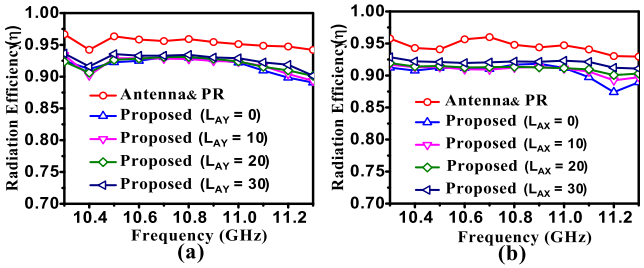

Fig. 15. Simulated radiation efficiency of the proposed configuration. (a) Case-I. (b) Case-II.

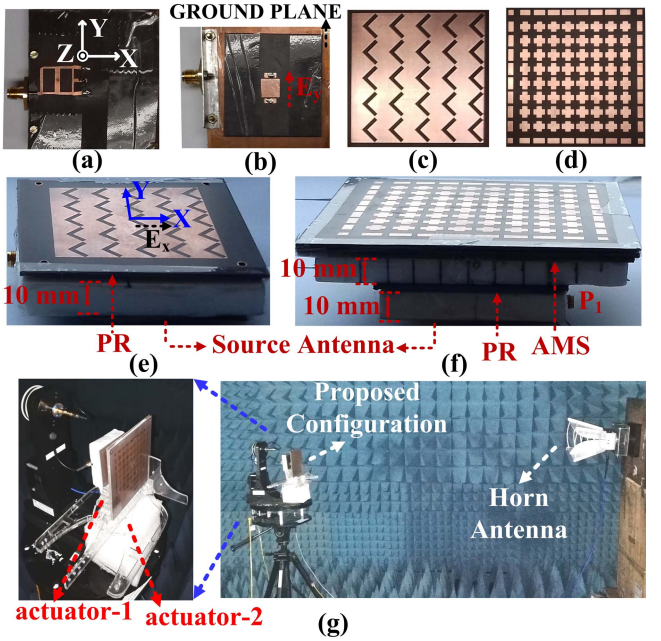

Fig. 16. Fabricated prototypes. (a) Back view of the source antenna. (b) Front view of the source antenna. (c) One layer of the PR. (d) One layer of the AMS lens. (e) Antenna subsystem (source antenna and PR). (f) Proposed configuration. (g) Measurement setup along with two actuators.

Here, a standard horn (LB-101180) of size 244 × 164 × 204 mm^3 is used as a transmitting antenna and the proposed configuration is placed at the receiving side, while satisfying the far-field condition. The proposed configuration with two actuators are shown in the inset. Here, source antenna, along with Layer-2 (printed on 0.51 mm-thick substrate, Sub-2) of the PR, is kept in a fixed position, whereas Layer-1 (printed on 1.58 mm-thick substrate, Sub-1) of the PR can be freely rotated around the axis of the source antenna using actuator-1. Therefore, this actuator can easily alter the relative orientations of the metallic layers of the PR in order to obtain either Y- or X-polarized EM waves at the output of the PR. Afterward, one additional actuator (actuator-2) is also adopted here for linearly varying the location of the AMS lens in-front of the antenna subsystem (source antenna and PR). This actuator-2 facilitates independent beam scanning of both orthogonally polarized fan-beam patterns. It is to be noted here that the proposed configuration neither generates nor steers these Y- and X-polarized fan-beams simultaneously. However, aforementioned in-plane translation of the AMS lens can steer either the Y-polarized (E_Y) fan-beam along the Y-direction or an X-polarized (E_X) fan-beam along the X-direction, depending on the state of the PR and direction of movement of the AMS lens. Therefore, with the help of two actuators, the proposed configuration can easily provide independent scanning of two orthogonally polarized fan-beam radiation patterns.

V. Conclusion

A novel AMS-based integrated antenna system capable of producing two orthogonally polarized fan-beam radiation patterns with independent beam-scanning performance has been demonstrated in this paper. The phase profile of the proposed AMS lens is obtained by combining two orthogonal cylindrical phase profiles in a single lens structure. A differentially driven, linearly polarized MPA has been used here to illuminate the AMS lens. This source antenna basically produces the beam in the broadside direction with low cross-polar radiation. The source antenna is loaded with a PR in order to independently obtain either Y-polarized (E_Y) or X-polarized (E_X) EM waves using one actuator. The antenna subsystem (source antenna and PR) has then been integrated with the newly designed AMS lens, which basically facilitates two orthogonally polarized fan-beam-type patterns with narrow beamwidth along the direction of their respective polarizations. Finally, the in-plane movement of the AMS lens with the help of one more actuator provides independent beam scanning of Y- and X-polarized EM waves in the YZ and XZ planes, respectively. The proposed structure is facilitating two orthogonally oriented fan-beam patterns with the orthogonal polarizations and independent beam-scanning ability. Moreover, problem of radiation blockage commonly appearing in the reflector antenna is not present in the proposed topology due to the transmitting characteristics of the AMS lens. Additionally, the absence of the complicated feed network and the simple fabrication process using the standard printed circuit board technology make the proposed AMS-based fan-beam configuration quite advantageous over similar types of structures reported earlier in the literature. The proposed compact integrated antenna system can potentially be used for various industrial applications such as in the imaging system and the radar configuration, where scanning of fan-beams with orthogonal polarizations is sometimes required at the transmitter and the receiver ends.

REFERENCES

[1] H. Lee, Y. H. Kim, V. A. Volkov, R. V. Kozhin, D. M. Vavriv, and T. S. Kim, "35 GHz compact radar using fan beam antenna array for obstacle detection," *Electron. Lett.*, vol. 43, no. 25, pp. 1461–1462, Dec. 2007.

[2] S. G. Hay, J. W. Archer, G. P. Timms, and S. L. Smith, "A beam-scanning dual-polarized fan-beam antenna suitable for millimeter wavelengths," *IEEE Trans. Antennas Propag.*, vol. 53, no. 8, pp. 2516–2524, Aug. 2005.

[3] S. G. Hay, S. L. Smith, G. P. Timms, and J. W. Archer, "Three-shaped-reflector beam-scanning pillbox antenna suitable for mm wavelengths," *IEEE Trans. Antennas Propag*, vol. 59, no. 7, pp. 2495–2501, Jul. 2011.

[4] S. Y. Eom *et al.*, "Design and test of a mobile antenna system with tri-band operation for broadband satellite communications and DBS reception," *IEEE Trans. Antennas Propag.*, vol. 55, no. 11, pp. 3123–3133, Nov. 2007.

[5] A. Falahati, M. NaghshvarianJahromi, and R. M. Edwards, "Wideband fan-beam low-sidelobe array antenna using grounded reflector for DECT, 3G, and ultra-wideband wireless applications," *IEEE Trans. Antennas Propag.*, vol. 61, no. 2, pp. 700–706, Feb. 2013.

[6] J. Kriz, V. Krcmer, J. Pidanic, and V. Schejbal, "Antenna beamwidth control [antenna designer's notebook]," *IEEE Antennas Propag. Mag.*, vol. 52, no. 1, pp. 163–170, Feb. 2010.

[7] R. M. Thompson, "Doppler-weather signal processing for a rapid RF- and PRF-agile airport surveillance radar," in *Proc. 19th Digit. Avionics Syst. Conf. (DASC)*, vol. 2, Oct. 2000, pp. 7C5/1–7C5/8.

[8] C.-A. Yu *et al.*, "24 GHz horizontally polarized automotive antenna arrays with wide fan beam and high gain," *IEEE Trans. Antennas Propag.*, vol. 67, no. 2, pp. 892–904, Feb. 2019.

[9] F. Sadjadi, M. Helgeson, J. Radke, and G. Stein, "Radar synthetic vision system for adverse weather aircraft landing," *IEEE Trans. Aerosp. Electron. Syst.*, vol. 35, no. 1, pp. 2–14, Jan. 1999.

[10] D. L. Runyon, "Optimum directivity coverage of fan-beam antennas," *IEEE Antennas Propag. Mag.*, vol. 44, no. 2, pp. 66–70, Apr. 2002.

[11] M. Imbert, J. Romeu, M. Baquero-Escudero, M. Martinez-Ingles, J. Molina-Garcia-Pardo, and L. Jofre, "Assessment of LTCC-based dielectric flat lens antennas and switched-beam arrays for future 5G millimeter-wave communication systems," *IEEE Trans. Antennas Propag.*, vol. 65, no. 12, pp. 6453–6473, Dec. 2017.

[12] N. Yu *et al.*, "Light propagation with phase discontinuities: Generalized laws of reflection and refraction," *Science*, vol. 334, no. 6054, pp. 333–337, Oct. 2011.

[13] N. Yu and F. Capasso, "Flat optics with designer metasurfaces," *Nature Mater.*, vol. 13, pp. 139–150, Jan. 2014.

[14] M. Li and N. Behdad, "Wideband true-time-delay microwave lenses based on metallo-dielectric and all-dielectric lowpass frequency selective surfaces," *IEEE Trans. Antennas Propag.*, vol. 61, no. 8, pp. 4109–4119, Aug. 2013.

[15] A. K. Azad, A. V. Efimov, S. Ghosh, J. Singleton, A. J. Taylor, and H.-T. Chen, "Ultra-thin metasurface microwave flat lens for broadband applications," *Appl. Phys. Lett.*, vol. 110, no. 22, 2017, Art. no. 224101.

[16] S. Yu, H. Liu, and L. Li, "Design of near-field focused metasurface for high-efficient wireless power transfer with multifocus characteristics," *IEEE Trans. Ind. Electron.*, vol. 66, no. 5, pp. 3993–4002, May 2019.

[17] K. K. Katare, S. Chandravanshi, A. Biswas, and M. J. Akhtar, "Realization of split beam antenna using transmission-type coding metasurface and planar lens," *IEEE Trans. Antennas Propag.*, vol. 67, no. 4, pp. 2074–2084, Apr. 2019.

[18] K. K. Katare, A. Biswas, and M. J. Akhtar, "Microwave beam steering of planar antennas by hybrid phase gradient metasurface structure under spherical wave illumination," *J. Appl. Phys*, vol. 122, no. 23, Nov. 2017, Art. no. 234901.

[19] K. K. Katare, A. Biswas, and M. J. Akhtar, "Wideband beam-steerable configuration of metasurface loaded slot antenna," *Int. J. RF Microw. Comput. Aided Eng.*, vol. 28, no. 8, 2018, Art. no. e21408.

[20] K. K. Katare, S. Chandravanshi, A. Biswas, and M. J. Akhtar, "A compact configuration of semicircular metasurface loaded slot antenna for beam steering application," *Int. J. RF Microw. Comput. Aided Eng.*, vol. 29, no. 2, 2019, Art. no. e21526.

[21] K. K. Katare, A. Biswas, and M. J. Akhtar, "Near-field phase modulation using a semicircular radially gradient metasurface for beam steering of an RF antenna," *J. Comput. Electron.*, vol. 18, no. 2, pp. 671–679, Jan. 2019.

[22] K. K. Katare, S. Chandravanshi, A. Biswas, and M. J. Akhtar, "Beam-switching of Fabry–Pérot cavity antenna using asymmetric reflection phase response of bianisotropic metasurface," *IET Microw., Antennas Propag.*, vol. 13, no. 6, pp. 842–848, May 2019.

[23] H. F. Ma, G. Z. Wang, G. S. Kong, and T. J. Cui, "Independent controls of differently-polarized reflected waves by anisotropic metasurfaces," *Sci, Rep.*, vol. 5, Jan. 2015, Art. no. 9605.

[24] K. Achouri, G. Lavigne, and C. Caloz, "Comparison of two synthesis methods for birefringent metasurfaces," *J. Appl. Phys.*, vol. 120, no. 23, 2016, Art. no. 235305.

[25] T. Cai *et al.*, "Ultra-thin polarization beam splitter using 2-D transmissive phase gradient metasurface," *IEEE Trans. Antennas Propag.*, vol. 63, no. 12, pp. 5629–5636, Dec. 2015.

[26] H. Markovich, D. Filonov, I. Shishkin, and P. Ginzburg, "Bifocal Fresnel lens based on the polarization-sensitive metasurface," *IEEE Trans. Antennas Propag.*, vol. 66, no. 5, pp. 2650–2654, May 2018.

[27] T. Cai, G.-M. Wang, X.-L. Fu, J.-G. Liang, and Y.-Q. Zhuang, "High-efficiency metasurface with polarization-dependent transmission and reflection properties for both reflectarray and transmitarray," *IEEE Trans. Antennas Propag.*, vol. 66, no. 6, pp. 3219–3224, Jun. 2018.

[28] F. Yang, R. Deng, S. Xu, and M. Li, "Design and experiment of a near-zero-thickness high-gain transmit-reflect-array antenna using anisotropic metasurface," *IEEE Trans. Antennas Propag.*, vol. 66, no. 6, pp. 2853–2861, Jun. 2018.

[29] Y. P. Zhang and J. J. Wang, "Theory and analysis of differentially-driven microstrip antennas," *IEEE Trans. Antennas Propag.*, vol. 54, no. 4, pp. 1092–1099, Apr. 2006.

[30] S. Chandravanshi, S. S. Sarma, and M. J. Akhtar, "Design of triple band differential rectenna for RF energy harvesting," *IEEE Trans. Antennas Propag.*, vol. 66, no. 6, pp. 2716–2726, Jun. 2018.

[31] M. Caillet, M. Clenet, A. Sharaiha, and Y. M. M. Antar, "A compact wide-band rat-race hybrid using microstrip lines," *IEEE Microw. Wireless Compon. Lett.*, vol. 19, no. 4, pp. 191–193, Apr. 2009.

[32] V. G. Kasabegoudar and K. J. Vinoy, "Coplanar capacitively coupled probe fed microstrip antennas for wideband applications," *IEEE Trans. Antennas Propag.*, vol. 58, no. 10, pp. 3131–3138, Oct. 2010.

[33] S. A. Winkler, W. Hong, M. Bozzi, and K. Wu, "Polarization rotating frequency selective surface based on substrate integrated waveguide technology," *IEEE Trans. Antennas Propag.*, vol. 58, no. 4, pp. 1202–1213, Apr. 2010.

[34] E. B. Lima, S. A. Matos, J. R. Costa, C. A. Fernandes, and N. J. G. Fonseca, "Circular polarization wide-angle beam steering at Ka-band by in-plane translation of a plate lens antenna," *IEEE Trans. Antennas Propag.*, vol. 63, no. 12, pp. 5443–5455, Dec. 2015.